Use of ScaRaB Measurements for Validating a GOES-Based TOA Radiation Product

ALEXANDER TRISHCHENKO AND ZHANQING LI

Canada Centre for Remote Sensing, Ottawa, Ontario, Canada

(Manuscript received 15 April 1997, in final form 14 October 1997)

ABSTRACT

Lack of calibrated radiation measurements at the top of the atmosphere (TOA) between major spaceborne radiation missions entails inference of the TOA radiation budget from operational weather sensors. The inferred data are subject to uncertainties due to calibration, narrow- to broadband conversion, etc. In this study, a surrogate TOA earth radiation budget product generated from *GOES-7* (Geostationary Operational Environmental Satellite) imagery data for use in the U.S. Atmospheric Radiation Measurement (ARM) program was validated using measurements from the ScaRaB radiometer flown on board the *METEOR-3/7* satellite. Comparisons were made between coincident and collocated shortwave and longwave radiative quantities derived from GOES and ScaRaB sensors over an ARM experimental locale in the South Great Plains of Oklahoma, during April and July 1994. The comparisons are proven to be instrumental in validating the calibration and narrow- to broadband conversion used to obtain broadband radiative quantities from GOES digital counts. Calibrations for both visible and infrared window channels have small uncertainties, whereas narrow- to broadband conversion of shortwave measurements contains large systematic errors. The caveat stems from use of a quadratic conversion equation instead of a linear one, as was found from ScaRaB narrow- and broadband measurements. The ensuing errors in the estimates of broadband albedo depend on scene brightness, underestimation for bright scenes, and overestimation for dark scenes. As a result, the magnitude of the TOA cloud radiative forcing is underestimated by about 14 W m^{-2} or 7.5% on a daytime mean basis. After correcting this error, the ratio of cloud radiative forcing (a measure of the impact of clouds on atmospheric absorption) derived from ARM measurements turns out to be 1.07, which is in even closer agreement with radiative transfer models than found from previous studies using original GOES products.

1. Introduction

Radiation budget at the top of the atmosphere (TOA) is an important boundary condition of the earth's climate system and is essential for studying the transfer of solar energy within the system. This boundary condition is characterized by three radiative variables, namely, the solar constant, broadband shortwave (SW) reflected flux or albedo, and the longwave (LW) irradiance emitted from the earth's system. Except for the first quantity that is more or less a ''constant,'' the other two vary considerably in time and space over a range of scales. Monitoring these changes is thus key to understanding the climate system and its dynamics at different spatial and temporal scales.

There have been several space missions dedicated to monitoring the TOA radiation budget (TRB). Most notable are the Nimbus series such as *Nimbus-3* (Raschke et al. 1973), *Nimbus-7* (Jacobowitz 1984), the Earth Radiation Budget Experiment (ERBE) (Barkstrom et al. 1986), the Scanner for Radiation Budget (ScaRaB) (Kandel et al. 1994), and the Clouds and the Earth's Radiant Energy System (CERES) (Wielicki et al. 1996). Notwithstanding, continuous observation of TRB over a long period of time, as required for climate studies, has been impeded by the data gaps existing between these missions. For example, since the ERBE scanners ceased functioning in 1990, there have been almost no radiation budget measurements by a scanning radiometer, except for only one year of observation by the ScaRaB. The dearth of TRB data during this period hinders the Atmospheric Radiation Measurement (ARM) program among others.

ARM is an experimental program sponsored by the U.S. Department of Energy. ARM field observation commenced in 1990 and is planned to last at least a decade. It may be the largest undertaking of experimental studies dealing with radiation and climate modeling. The main objectives of ARM are to improve the understanding of processes governing atmospheric radiation and the description of these processes in climate models (Stokes and Schwartz 1994). To this end, several clouds and radiation testbeds (CARTs) were deployed in three locales with distinct climate regimes. Extensive measurements are collected from ground-based, airborne, and spaceborne instruments of radiative fluxes and parameters modifying the transfer of radiation. Lack

Corresponding author address: Dr. Z. Li, Canada Centre for Remote Sensing, 588 Booth St., Ottawa, ON K1A 0Y7 Canada.
E-mail: Zhanqing.Li@CCRS.NRCan.gc.ca

TABLE 1. Characteristics of the ScaRaB radiometer.

Parameter	Value
Number of channels	4
Spectral intervals	
Visible channel	0.55–0.65 μm
Solar channel	0.2–4 μm
Total channel	0.2–>50 μm
IR window channel	10.5–12.5 μm
Scanning mode	Cross track
Number of pixels per line	51
Cycle duration	6 s
Pixel measurement time	62.5 ms
Field of view	48 × 48 mrad
Pixel size at nadir	60 km × 60 km
Angular distance between pixel centers	1.95°
Scanning angle limits	±49°

of direct TOA radiation measurements necessitates the creation of a surrogate TRB dataset from Geostationary Operational Environmental Satellite (GOES) weather satellites (Minnis et al. 1995). These data are valuable to many ARM investigations and have been employed in addressing such critical issues as the cloud absorption anomaly (Imre et al. 1996). However, since the GOES visible narrowband sensor was not calibrated, the quality of the inferred broadband data is open to question without a proper validation (Cess et al. 1996).

A validation is presented here of the GOES-based TRB dataset for the Southern Great Plains (SGP) CART site using ScaRaB measurements. Two major potential sources of uncertainty, namely, calibration and narrowband to broadband conversion are examined. The calibration issue was addressed by comparing coincident and collocated measurements in the narrowband channels of a noncalibrated GOES radiometer and a calibrated ScaRaB radiometer. Narrowband to broadband conversion is assessed by comparing the conversion relationships used in generating the TRB data from GOES and obtained from the ScaRaB narrow- and broadband measurements. The characteristics of these radiometers are described in section 2. Data and various corrections are discussed in section 3. Section 4 presents the results of validations for calibration and narrow- to broadband conversion. The impact of the errors found from the validations on TRB and cloud radiative forcing is also addressed. Summary of the study is presented in section 5.

2. Radiometers

a. ScaRaB/METEOR-3/7

ScaRaB is a space mission conducted jointly by France, Russia, and Germany (Kandel et al. 1994). The first ScaRaB was launched on board the Russian *METEOR-3/7* satellite, and the second one is planned for 1998. ScaRaB/*METEOR-3/7* operated from February 1994 through March 1995. The *METEOR-3/7* satellite revolved about 1200 km above the earth on a nonsun-

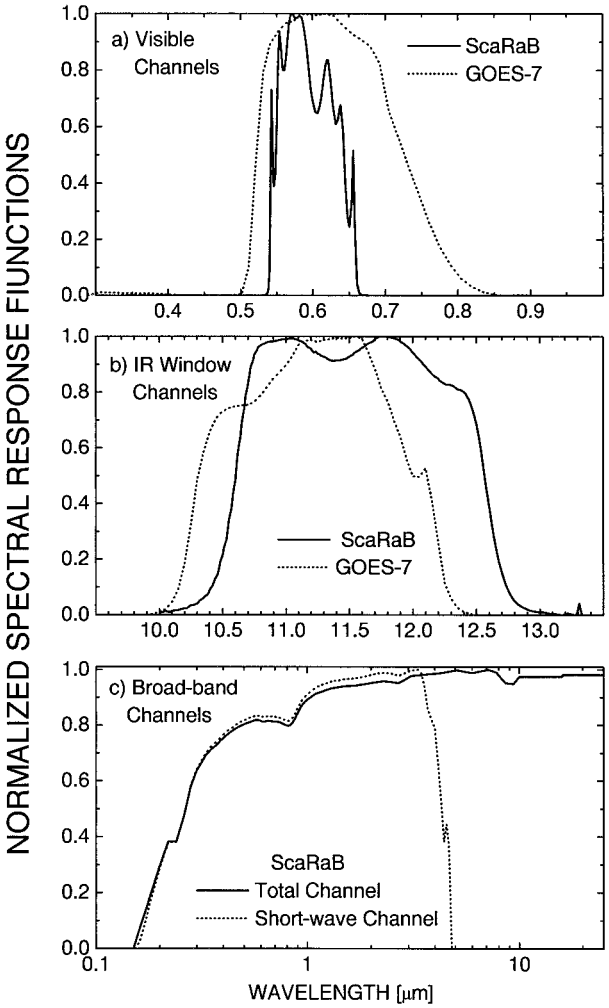

FIG. 1. Normalized spectral response functions for ScaRaB and *GOES-7* VISSR radiometers in (a) visible channels, (b) IR window channels, and (c) broadband ScaRaB channels.

synchronous orbit with a 82.5° inclination angle. The total period of satellite orbit precession with respect to the sun was approximately seven months, during which ScaRaB provided measurements at all local solar times for both ascending and descending orbits. Table 1 delineates some parameters of the ScaRaB radiometer, including its four channels: visible (VIS, 0.55–0.65 μm), shortwave (SW, 0.2–4 μm), total (TOT, 0.2–>50 μm), and infrared window (IRW, 10.5–12.5 μm). The normalized spectral response functions of the four channels are shown in Fig. 1, in comparison with that of the *GOES-7* sensor. The field of view (FOV) of a nadir ScaRab pixel is about 60 km × 60 km.

ScaRaB has an onboard calibration system using multiple sources. They include the blackbody (BB) simulators for channels 3 (LW part) and 4 (IR window) and three sets of lamps for channels 1 (VIS), 2 (SW), and 3 (SW part). The visible channel was calibrated once every 2 weeks with one lamp (L11). The SW calibration

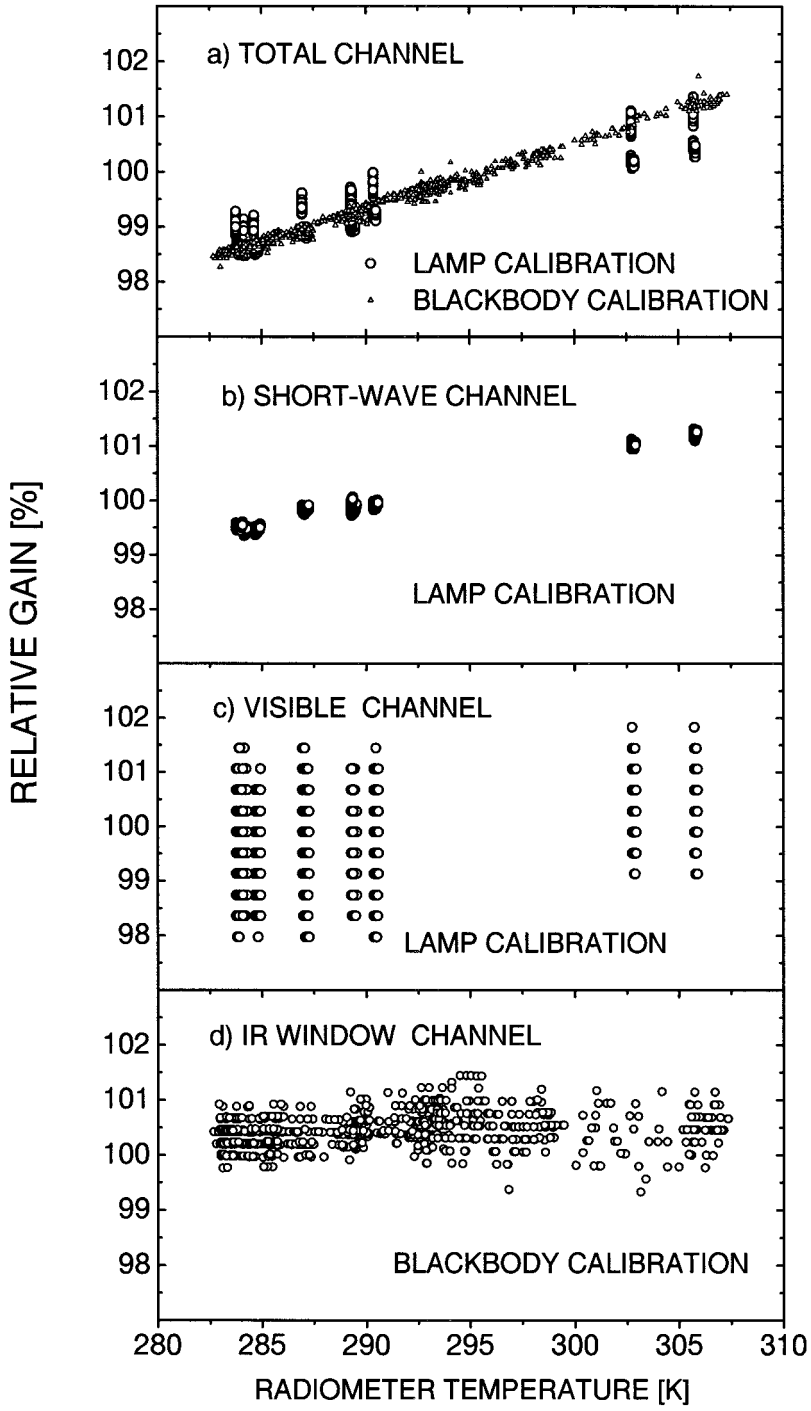

FIG. 2. Variations of relative ScaRaB channel gains with radiometer temperature for (a) total channel, (b) shortwave channel, (c) visible channel, and (d) IR window channel. The sources of calibration are marked on the plots.

was done twice a day with one lamp and twice a month with another lamp. The SW part of the TOT channel was calibrated twice a month. The IR window channel and the LW part of the TOT channel were calibrated every 12 s. The results of onboard calibration in terms of relative calibration gains are shown in Fig. 2. Relative gains were determined from measurements made during calibration mode and the nominal calibration parameters listed in Monge et al. (1994). For most channels, they vary linearly with the temperature of radiometers that

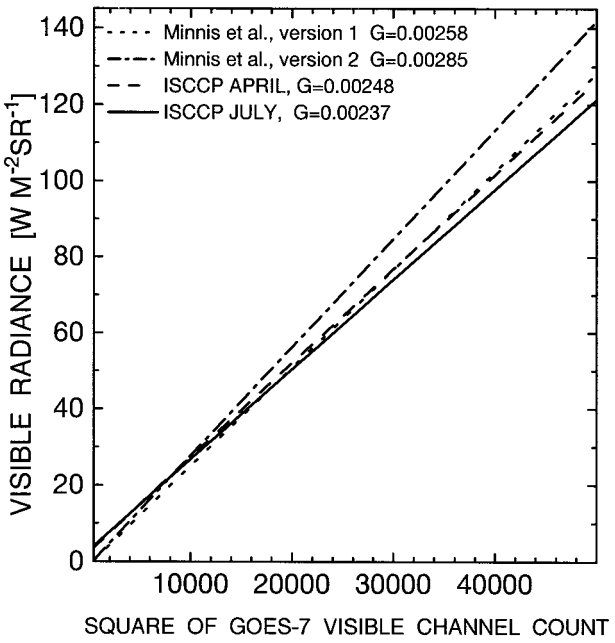

FIG. 3. A comparison of ISCCP and NASA LaRC calibration for *GOES-7* VISSR visible channel. Plotted are the gains (G; W m^{-2} sr^{-1}) used in two versions of the *GOES-7* data generated by Minnis et al. (1995) and two months used in ISCCP.

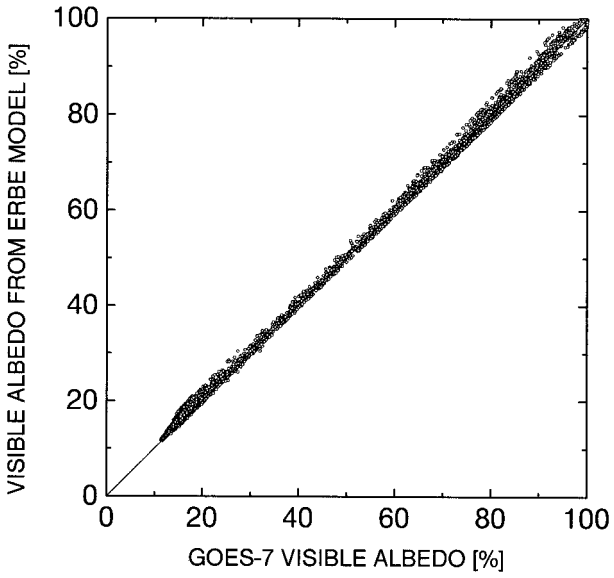

FIG. 4. A comparison of ERBE and GOES angular dependence models applied to *GOES-7* VISSR visible reflectance measurements. The mean difference and standard deviation are 0.34% and 0.85%, respectively.

were monitored on board. Such a temperature dependence was taken into account in calibration. The temperature drift is more important for the TOT channel than for the other channels. Note the consistency between different methods of calibration for the TOT channel based on lamp sources and on a BB simulator (Fig. 2a). Comparison of the calibrations for the TOT channel with a BB and a lamp, and for the SW channel with two lamps, demonstrates that the accuracy of calibration is generally within 0.2%–0.5% after the temperature dependence is removed, provided that the lamp luminosity is stable. It is less accurate for the VIS channel but still within 1%–2%.

The accuracy of ScaRaB flux data was also evaluated by comparing synchronous measurements from the Earth Radiation Budget Satellite (ERBS) wide-field-of-view (WFOV) radiometer and from the ScaRaB scanning radiometer (Bess et al. 1997). The agreement is remarkably close, the mean differences being within 0.76 W m^{-2} for SW and 0.55 W m^{-2} for LW at night and 3.8 W m^{-2} during daytime, and the standard deviations being 5.5 W m^{-2} for SW and 1.9 and 2.3 W m^{-2} for nighttime and daytime LW measurements. The agreement is comparable to that between the ERBE scanner and nonscanner observations (Green et al. 1990).

b. *VISSR*/GOES-7

The Visible and Infrared Spin-Scan Radiometer (VISSR) on board *GOES-7* did not have in-flight cali-

TABLE 2. Statistics of the comparison of cloud classification by ScaRaB and *GOES-7*. The first and second values appearing in the table correspond to the numbers of all matched pixels and only those with ScaRaB VZA less than 25°.

	ScaRaB			
GOES-7	CLR	PC	MC	OVR
		April, daytime		
CLR	900/603	269/50	6/0	0/0
PC	259/166	422/161	11/3	0/0
MC	36/23	262/122	88/30	1/0
OVR	21/11	359/128	1036/404	886/376
		April, nighttime		
CLR	124/20	1547/523	150/92	1/0
PC	2/1	186/64	85/50	0/0
MC	3/2	127/66	44/20	1/1
OVR	16/10	670/408	1164/615	979/530
		July, daytime		
CLR	77/53	43/30	0/0	0/0
PC	14/8	42/25	2/0	0/0
MC	11/6	26/13	11/8	0/0
OVR	1/0	8/6	21/9	40/6
		July, nighttime		
CLR	8/5	22/17	0/0	0/0
PC	1/0	10/7	1/1	0/0
MC	0/0	2/0	1/0	11/1
OVR	0/0	0/0	3/1	8/2
		All cases		
CLR	1109/681	1881/620	156/92	1/0
PC	276/175	660/257	99/54	0/0
MC	50/31	417/201	144/58	14/2
OVR	38/21	1037/542	2224/1029	1913/914

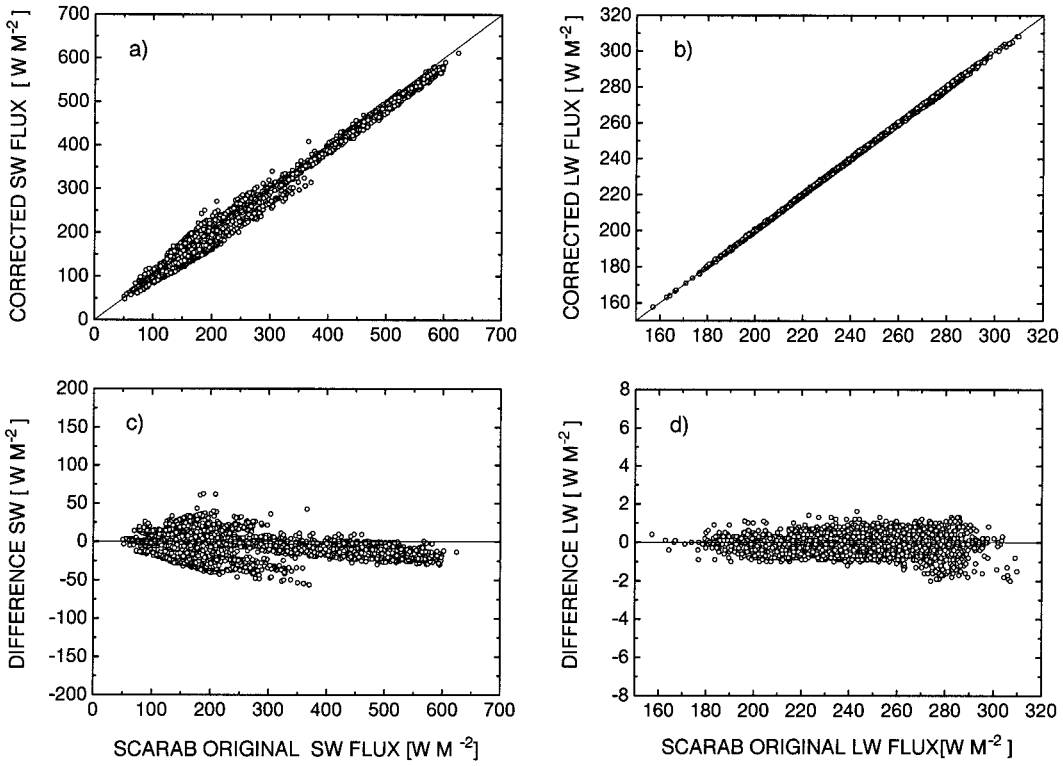

FIG. 5. A comparison of broadband fluxes derived according to ScaRaB and GOES cloud classification schemes for [(a) and (c)] SW and [(b) and (d)] LW components. Daytime data in April and July 1994 were used.

bration for the visible channel. Calibration of the GOES visible measurements is usually based on an intercomparison with National Oceanic and Atmospheric Administration/Advanced Very High Resolution Radiometer (NOAA/AVHRR) that is calibrated with reference to some relatively stable targets such as deserts or in comparison with radiative transfer calculations (Whitlock et al. 1990; Rossow et al. 1992; Rossow et al. 1995; Rao and Chen 1994; Minnis et al. 1995). GOES visible calibration is given by the following equation:

$$L = GD^2 - C, \tag{1}$$

where L is the filtered radiance (W m^{-2} sr^{-1}) over the visible band and D is the 8-bit digital count. Due to the lack of consensus on calibration, the values of gain (G) and offset (C) vary among users and are subject to change with time (Rossow et al. 1992; Rossow et al. 1995). For example, Fig. 3 shows four sets of calibration applied to *GOES-7*, including two versions used in generating the GOES product and two used in the International Satellite Cloud Climatology Project (ISCCP) (Rossow et al. 1992; Rossow et al. 1995). The large range of discrepancy constitutes a major source of uncertainty in deriving L. This study tests primarily the new calibration (version 2) used by Minnis et al. (1996). Unlike the visible channel, the GOES IRW channel has an onboard calibration. Therefore, the brightness temperature was derived following the instrument calibration that assumed a central wavelength at 11.5 μm, which results in an uncertainty less than 1 K.

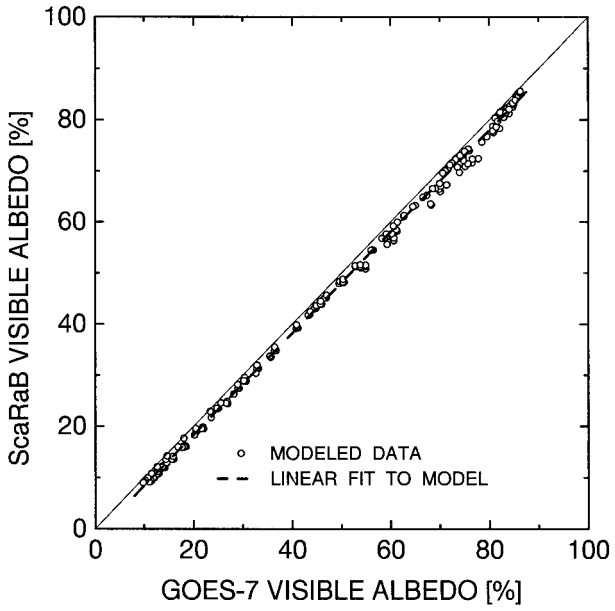

FIG. 6. Modeled relationship between ScaRaB and *GOES-7* visible TOA albedos over the SGP/CART site.

GOES data have a spatial resolution at nadir of about 1 km for the visible channel and 4 km for the IRW

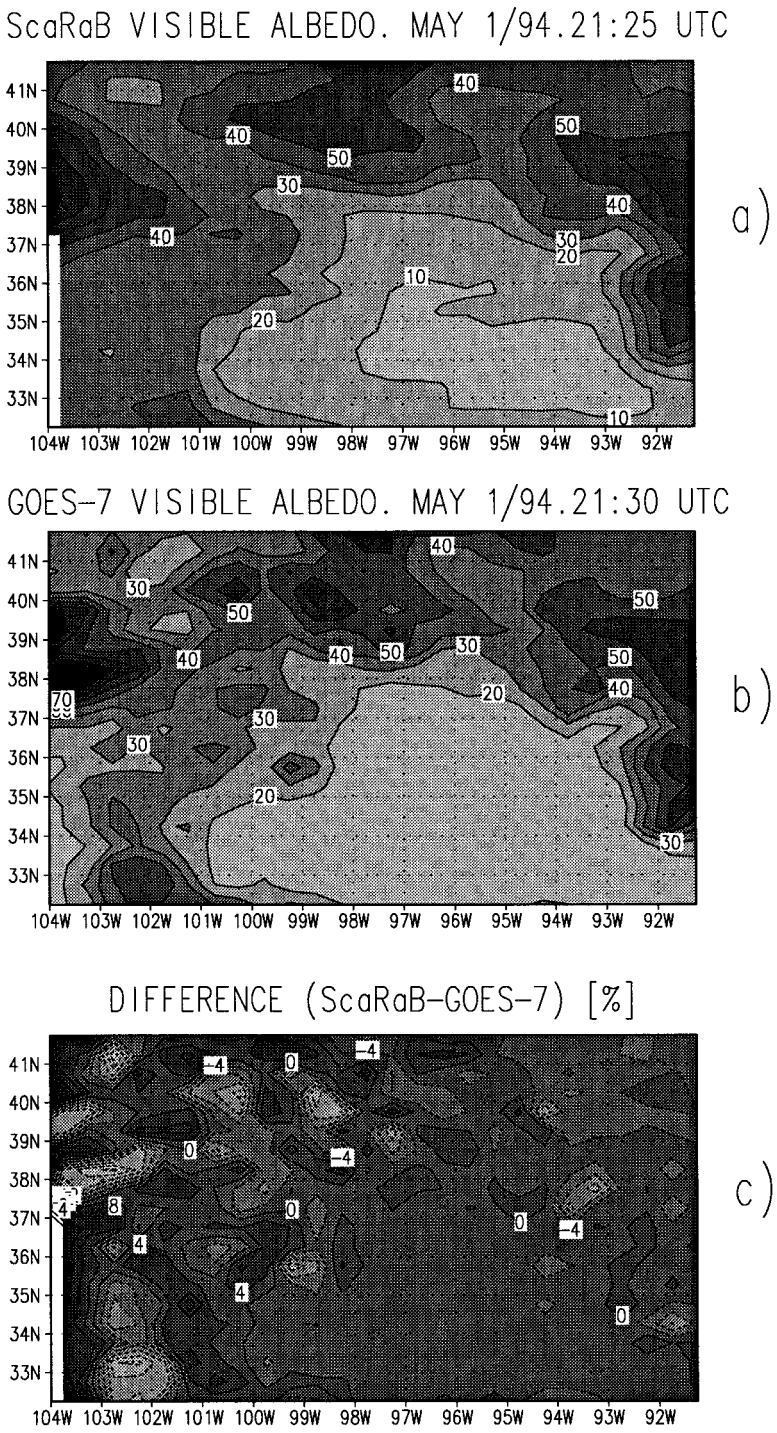

FIG. 7. The images of visible albedo measured by ScaRaB at a (a) full resolution, and by (b) *GOES-7* at a reduced resolution, and (c) their difference, over the ARM Southern Great Plain region on 1 May 1994 at 2130 UTC (*GOES-7*) and 2125 UTC (ScaRaB).

channel. However, reduced spatial resolution data of 0.5° × 0.5° and 0.3° × 0.3° (latitude and longitude) generated by Minnis et al. (1995) for the ARM program are used here.

3. Data and corrections

Data employed in this study essentially cover two months: April and July 1994. A small amount of data

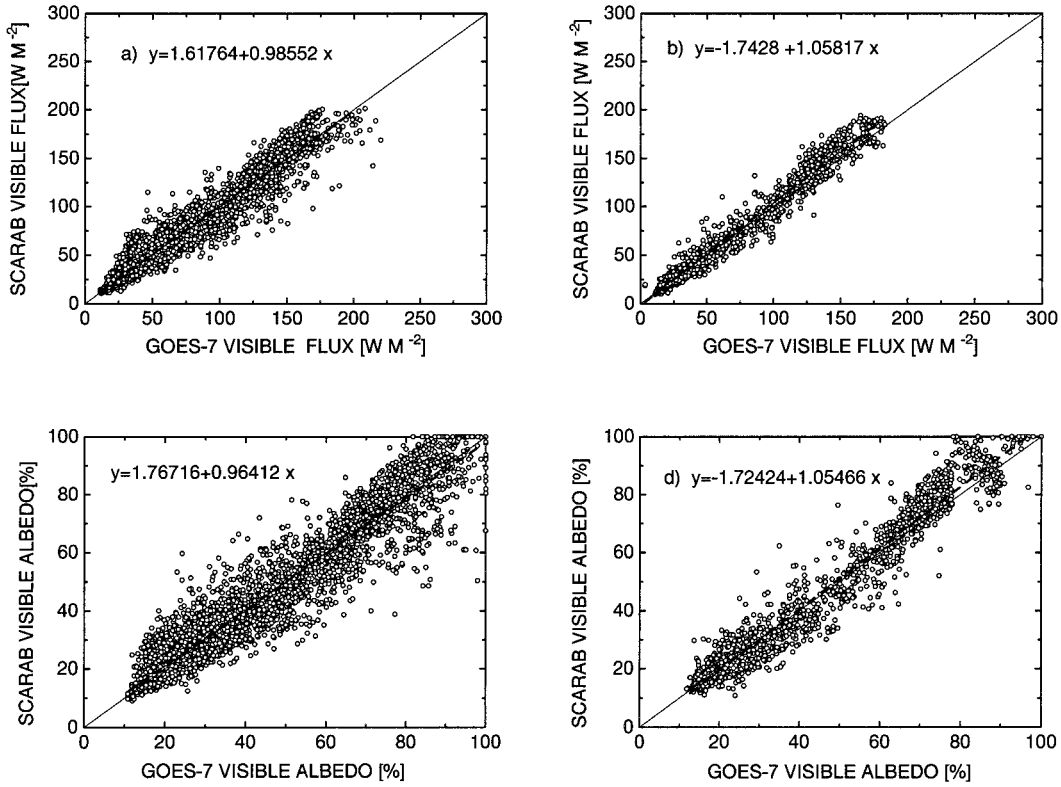

FIG. 8. Comparison of [(a) and (b)] visible fluxes and [(c) and (d)] albedos from ScaRaB and *GOES-7* for all matched data in April 1994 [(a) and (c)] and only those with the viewing zenith angle for ScaRaB less than 25° [(b) and (d)]. Linear regressions between the two quantifies under comparison are given in dashed lines.

from other months was also occasionally used. *GOES-7*-derived data were available via the World Wide Web (WWW) from the National Aeronautics and Space Administration (NASA)/Langley Research Center. They include TRB, visible and broadband albedos, IR window brightness temperature, cloud parameters, etc. The 0.5° spatial resolution data are employed as they are more comparable to the FOV of ScaRaB pixel data. Data of the latest versions effective as of submission of this manuscript were analyzed. For April 1994 data, it was the version released on 29 August 1996 and for July 1994 it was the version last modified on 6 May 1996. The April data encompass an area of $10° \times 14°$ over the SGP CART site, whereas the July data cover a much smaller area of $2.5° \times 2.5°$. As a result, the data volume in April is much larger than in July.

ScaRaB A2 data were matched to the *GOES-7* data. The A2 contains individual ScaRaB pixel measurements of the TOA radiance and irradiance, as well as scene identification and georeferencing information. The July ScaRaB data (version 6) were received from the Centre National Études Spatiales (CNES), Toulouse, France. The April data were processed by the Laboratoire de Météorologie Dynamique, Paris, France. Data from GOES and ScaRaB were matched under the following constraints.

1) Observation time difference was less than 15 min.
2) Distance between the centers of ScaRaB pixels and GOES grid cells was less than 20 km.
3) Difference in solar zenith angle was less than 2.5°.

After being matched, the data are subject to a series of corrections to account for discrepancies in viewing geometry, scene identification, and spectral coverage.

a. Angular correction

Reflected solar radiation is known to depend strongly on viewing direction. Such an angular dependence renders the comparison of radiance measured from two platforms difficult. A geostationary satellite observes a specific location at a constant viewing zenith angle (VZA), whereas the solar zenith angle (SZA) and relative azimuth angle (RAA) vary during the day. In contrast, a polar orbiting satellite observes fixed surface targets from different VZAs with relatively small changes in the SZA and RAA. Consequently, there are very few coincident and collocated measurements from *GOES-7* and ScaRaB with the same viewing geometry. The problem is alleviated if a comparison is made for albedo or irradiance (flux) defined over all viewing di-

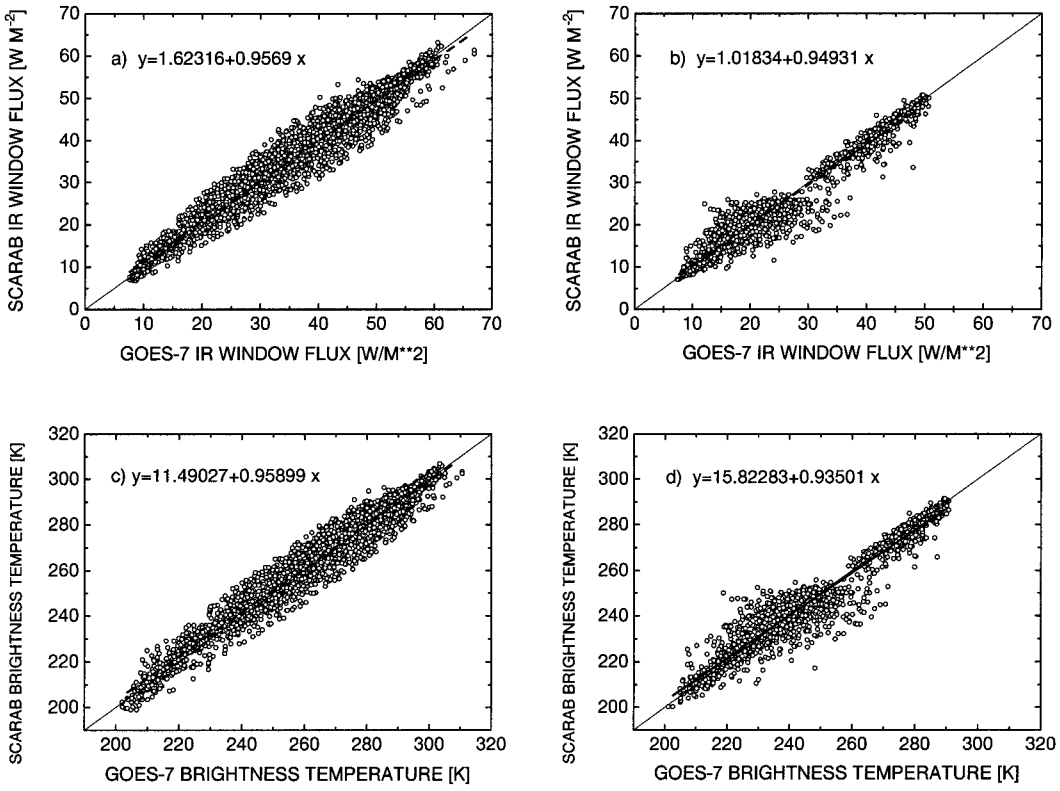

FIG. 9. Similar to Fig. 8 but for [(a) and (b)] IR window fluxes and [(c) and (d)] brightness temperatures for April and July observed during daytime [(a) and (c)] and nighttime [(b) and (d)]. The linear fits to the data are shown in dashed lines.

rections, rather than comparing reflectance or radiance observed from a monodirection.

The angular dependence model (ADM) used by ScaRaB (Viollier et al. 1995) to convert radiance into irradiance is the same as that used for ERBE (Suttles et al. 1988). However, the GOES-based TRB data (Minnis et al. 1995) were derived using a different ADM (Minnis and Harrison 1984; Minnis et al. 1991). A comparison of the albedos computed with the two different ADMs is shown in Fig. 4. The difference is small, indicating that the two ADMs are similar in effect. The resemblance between the two sets of ADMs is not sufficient, however, to warrant a valid comparison, unless both are also adequate. Use of an inadequate ADM may result in different albedos for a given scene viewed from different directions. The validity of the ERBE ADM has been addressed previously (e.g., Suttles et al. 1992; Li 1996; Ye and Coakley 1996). Here, we conducted an additional test by analyzing the variation of albedo with viewing angles over a fixed site in the SGP, as was done by Li (1996). No significant dependence was found beyond the natural variability of the scenes.

b. Scene correction

Since the ADMs are scene dependent (Suttles et al. 1988), a proper angular correction also relies on adequate scene identification. The ScaRaB scene identification scheme is the same as the ERBE one, namely, the maximum likelihood estimation (MLE) (Wielicki and Green 1989). While the scene pertains to both surface and sky conditions, only cloud determination is of concern here since the surface is fixed (land). Table 2 presents the statistics of a comparison of cloud classification according to ScaRaB and *GOES-7*. Overall, only about 38% of the cases in which clear and overcast scenes dominate have identical cloud classification; 49% are misclassified by one class. During daytime, the agreement is better, with 53% and 36% being classified equally and differed by one class, respectively. For partially cloudy (PC) and mostly cloudy (MC) scenes, the two classification schemes differ the most. The daytime cloud classification results obtained from *GOES-7* were compared with ARM ground observations and good agreement was found (Minnis et al. 1995). Cloud identification based on broadband measurements of coarse resolution is generally less reliable than that based on narrowband cloud imaging data of higher resolution (Diekmann and Smith 1989; Li and Leighton 1991). Misidentification of scene type may lead to significant errors in the ensuing fluxes estimated from radiance measurements. Therefore, ScaRaB fluxes were recalculated based on the scenes determined by *GOES-7*.

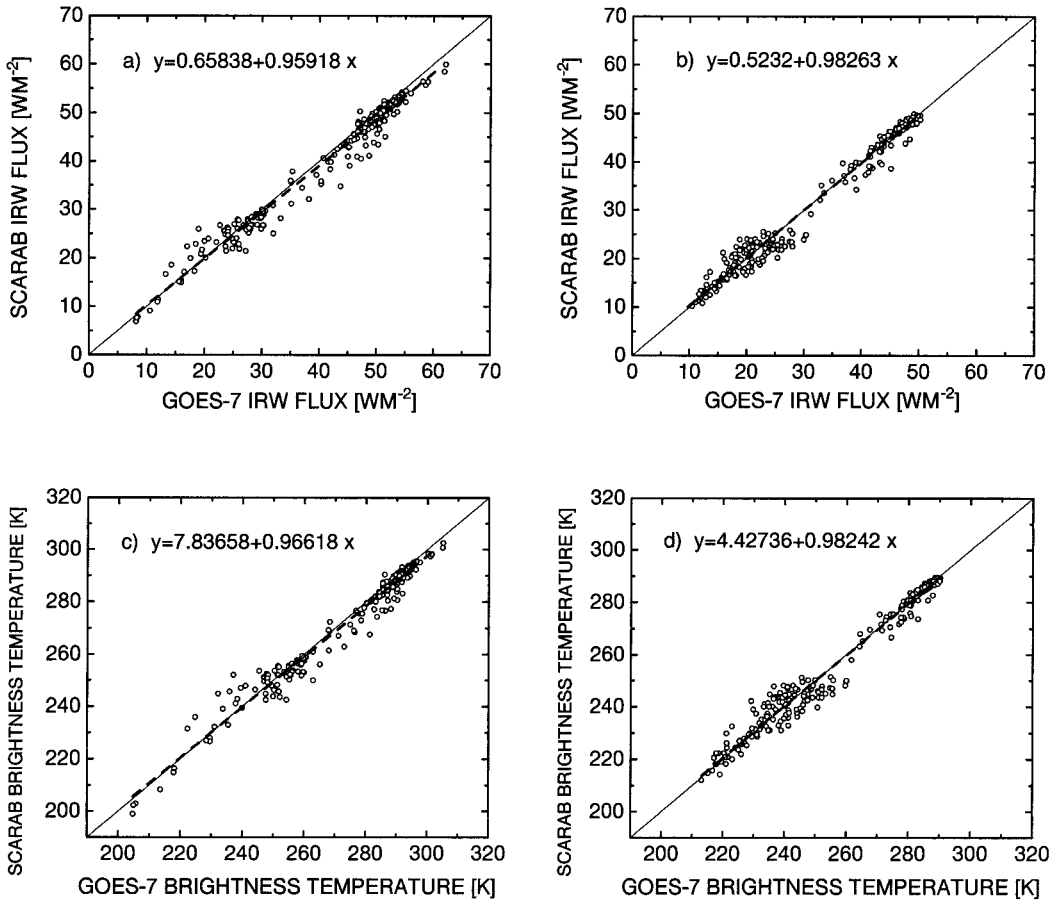

FIG. 10. Similar to Fig. 9 but for identical scenes determined by ScaRaB and *GOES-7* with close viewing zenith angles (differences of less than 5°).

During nighttime, analysis is restricted to the scenes that were equally identified by *GOES-7* and ScaRaB, considering that both ScaRaB and GOES scene identifications are less reliable. Figure 5 shows the differences in SW and LW fluxes due to the change of scene identification. For LW fluxes, the maximum difference is less than 2 W m^{-2} and the mean difference is close to 0. In contrast, the differences are substantial for SW fluxes with a maximum difference up to 70 W m^{-2}.

c. Spectral correction

Due to the difference in spectral response between the visible channels of *GOES-7* and ScaRaB (cf. Fig. 1), measurements from the two radiometers over the same scenes are not identical. To account for this discrepancy, model simulations were conducted with a radiative transfer model (Masuda et al. 1995). Two atmospheric profiles were used, namely, the standard midlatitude summer (MLS) atmosphere and the U.S. Standard Atmosphere, 1976, that are contained in the LOWTRAN-7 code (Kneizys et al. 1988). The continental type of aerosol with optical thickness ranging from 0.056 to 0.45 at 550 nm is included. Surface spectral and angular models were adopted from Rutan and Charlock (1997) for savannah and grassland. The model clouds of St, Sc, Cu, and Nb (Stephens 1978) were assumed with varying optical thickness (5–200) and altitudes (1–9 km). The modeled spectral reflectance data and the spectral response functions of GOES and ScaRaB radiometers were convolved. Simulated visible measurements for the two instruments are compared in Fig. 6. ScaRaB visible albedo appears to be systematically less than *GOES-7* visible albedo by about 1.5%–2%. The difference can be corrected by the following regression:

$$\alpha_{\mathrm{ScaRaB}} = -1.555\% + 0.994\alpha_{\mathrm{GOES\text{-}7}}. \qquad (2)$$

In comparison, the brightness temperatures derived from the infrared window channels of *GOES-7* and ScaRaB are very similar. Note that brightness temperature is determined at 11.5 μm, following the method of Minnis et al. (1995). Therefore, no correction was applied to the IRW measurements.

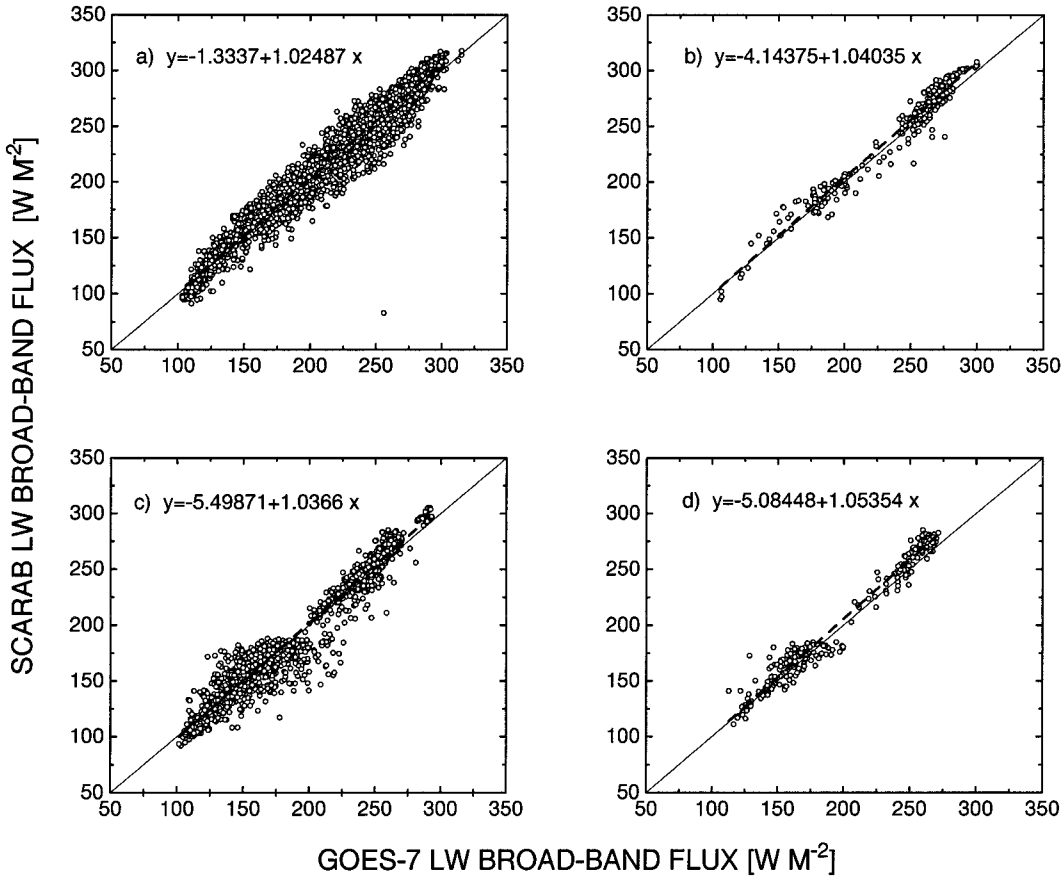

FIG. 11. Comparisons of longwave broadband fluxes observed by ScaRaB and estimated from *GOES-7* IR window measurements during [(a) and (b)] daytime and [(c) and (d)] nighttime for all matched data [(a) and (c)] in April and July and only those of similar VZA (difference of less than 5°) with identical scene types determined by ScaRaB and *GOES-7* [(b) and (d)].

4. Validation

a. Calibration

After data are matched and corrected, validation of calibration was done by comparing narrowband measurements from ScaRaB and *GOES-7*. The images of visible albedo are shown in Fig. 7 for (a) ScaRaB, (b) *GOES-7*, and (c) their differences. The two images were taken almost simultaneously with a time difference of merely 5 min. Overall, the two images match well, but they do differ in detailed features over some portions of the images, as is seen from Fig. 7c. This results from a combination of the discrepancy in image resolution and scene variability. Recall that the GOES image has a uniform resolution of 0.5° × 0.5° in latitude and longitude, whereas the FOV of ScaRaB pixel varies from 60 km at nadir to more than 150 km for extreme viewing angles. As a result, the GOES image exhibits more spatial variation than the ScaRaB image does, especially near the image edges where the spatial resolution difference reaches maximum and clouds happen to be more variable. Comparisons of individual pixel/grid data are shown in Fig. 8 for April 1994 for all the matched data (left panels) and only those of comparable spatial resolutions between *GOES-7* and ScaRaB data (right panels). The latter were obtained by restricting the VZAs of ScaRaB measurements to less than 25° so that the FOVs of the ScaRaB data retained are less than 75 km. The comparison of all matched data shows that there are good agreements in both albedos and fluxes, albeit large scattering. The mean difference is less than 2% in absolute albedo units. When the data of similar resolutions are compared, the scattering of the comparison is reduced substantially and a small systematic deviation from the 1:1 line is observed for larger albedo values. It should be pointed out that, due to the orbital constraints, the comparison shown in Fig. 8 is limited to relatively low fluxes, given that the maximum potential value for reflected flux is about 300 W m^{-2}. This is partially because the minimum solar zenith angle for the matched data is around 40°. If the trend discernible from Fig. 8b is true, visible fluxes or albedos of large magnitude may be underestimated by 2% to 3% because of improper *GOES-7* VISSR calibration.

A comparison of brightness temperature images between ScaRaB and *GOES-7* (not shown) is closer, al-

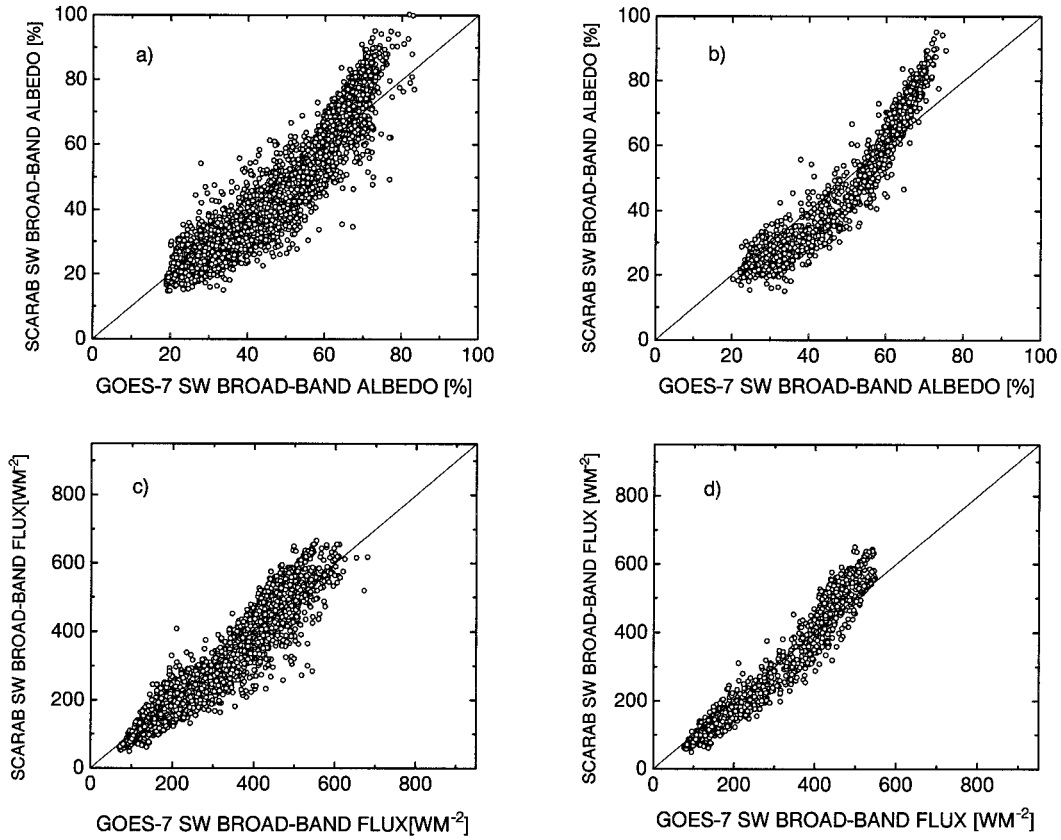

FIG. 12. Comparisons of [(a) and (b)] shortwave albedos and [(c) and (d)] fluxes observed with a ScaRaB broadband radiometer and estimated from *GOES-7* visible albedos for April and July 1994.

though similar in pattern, to Fig. 7. This is seen more clearly in the pixel comparison shown in Fig. 9 during daytime (left panels) and nighttime (right panels) for both months. Good agreements are found for both daytime and nighttime comparisons. The scattering stems partially from match-up errors in space and time and partially from an imperfect angular correction, in addition to a difference in spatial resolution. Since the ADM in the thermal band is primarily a function of viewing the zenith angle, an additional comparison is made with a constraint that the viewing zenith angles of ScaRaB and GOES data do not differ by more than 5°. The new comparison presented in Fig. 10 is apparently improved relative to Fig. 9, implying that a deficient angular correction does contribute to the difference between ScaRaB and *GOES-7* data. The narrowband IR window fluxes shown in Figs. 9 and 10 were calculated following the definition of Minnis et al. (1991) with a correction.[1]

[1] Note that there appears to be a typo in the use of their limb-darking function (Minnis et al. 1991; Minnis et al. 1995) for computing radiances at the nadir. Application of their method as printed in the literature produces results at variance with their data, which can, however, be reproduced exactly by using the inverse of the limb-darking function.

b. Narrowband to broadband conversion

The GOES-based broadband TOA fluxes were derived from narrowband measurements following a narrowband to broadband conversion. The performance of the conversion can be evaluated by comparing broadband quantities estimated from *GOES-7* and measured by ScaRaB.

The comparison of broadband LW fluxes is presented in Fig. 11 for all matched data (left panels) and those having similar VZAs with the same scenes identified by ScaRaB and *GOES-7* (right panels). There seems to be no significant difference, but there is a weak trend. The *GOES-7* technique tends to under- and overestimate LW flux for warm and cold scenes, respectively.

Shortwave comparison is shown in Fig. 12. The most striking feature of the albedo comparison is a curved trend deviated from 1:1 line. The trend indicates that the GOES-based shortwave broadband albedos are systematically lower than those measured by ScaRaB for highly reflective scenes (albedo greater than approximately 60%), and the opposite is the case for relatively dark scenes. The trend is less obvious for fluxes because a large number of data points of high albedos were observed at low sun angles. The absolute difference in albedo is from 15% to 20%. For thick clouds at local

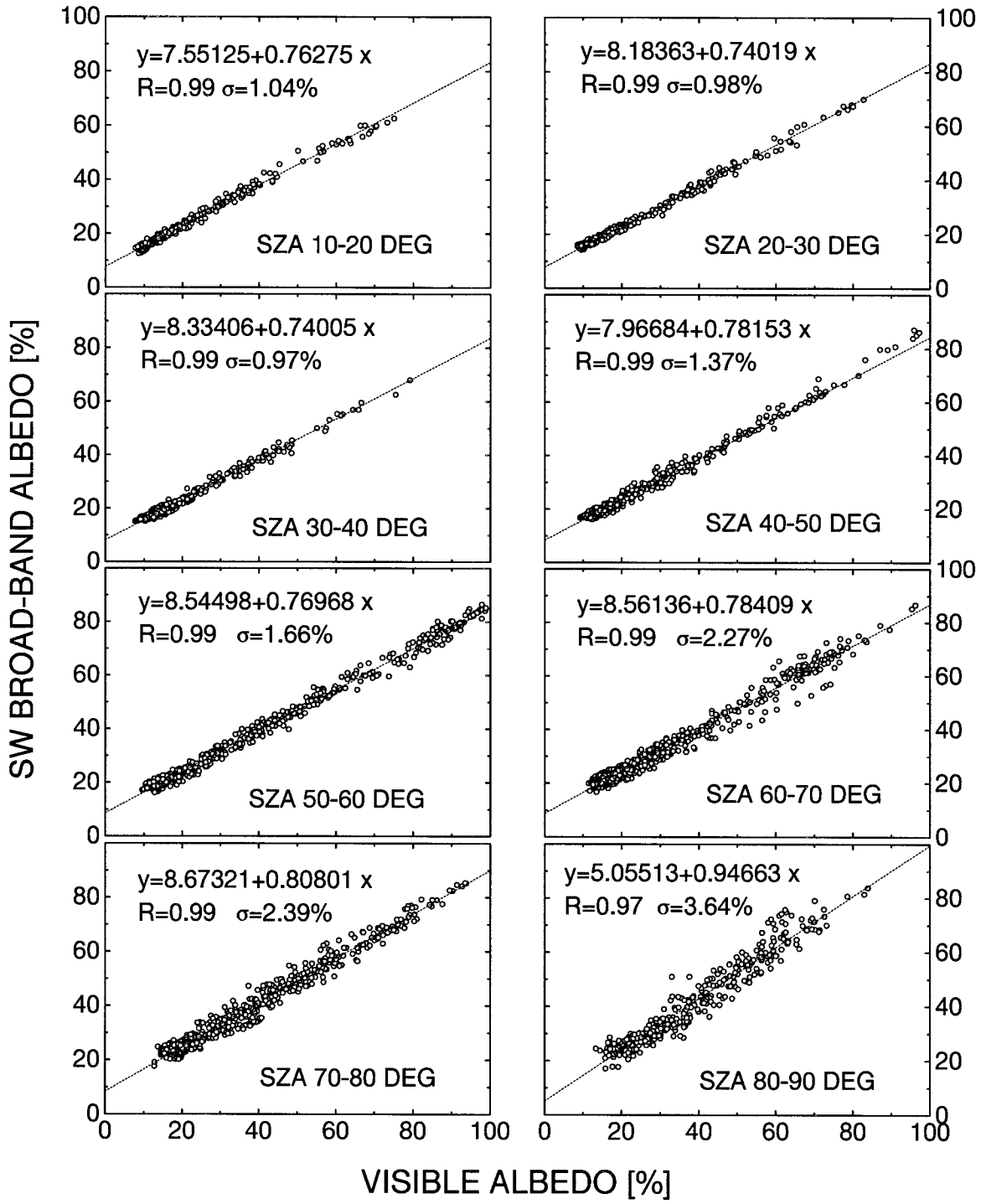

FIG. 13. Relationships between visible narrowband and SW broadband albedos for different ranges of the solar zenith angle (SZA). Both the visible and SW albedos were taken from ScaRaB radiometer over the SGP/ARM locale (35.61°–37.61°N, 96.5°–98.5°W) between March and August 1994. Open circles are observations and dotted lines correspond to linear fits to the data for each SZA bin. Regression correlation coefficients (R) and standard deviations (σ) are also given.

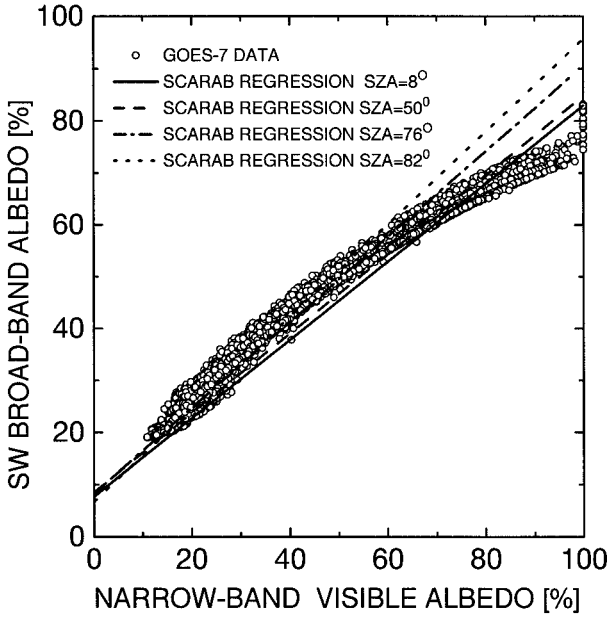

FIG. 14. Comparison of the relationship between narrow- and broadband albedos used for *GOES-7* and derived from ScaRaB measurements. Open circles denote broadband albedos derived from *GOES-7* algorithm adjusted to ScaRaB visible band using Eq. (2). The lines represent regressions obtained from ScaRaB, as given by Eq. (3), for various values of the SZA.

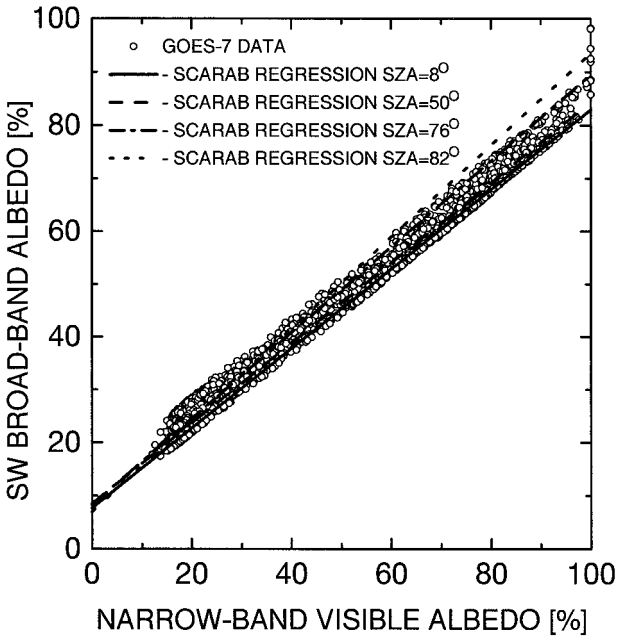

FIG. 15. Same as Fig. 14 but with a newly modified GOES product.

solar noon, this could result in an error in the estimation of TOA reflected fluxes of up to 200 W m^{-2}. For lower albedo values (less than approximately 60%), the GOES-based estimates of broadband albedo tend to be larger than ScaRaB measurements.

In addition to the calibration of GOES VISSR visible measurements that exhibits a weak trend of the same nature (cf. Fig. 8d), narrowband to broadband conversion appears to dominate the discrepancy revealed here. This is clear from a comparison of the conversion relationship used in generating the GOES broadband data with that obtained directly from ScaRaB visible and broadband SW observations. Shown in Fig. 13 is the visible–SW albedo relationships derived from ScaRaB measurements made over a $2° \times 2°$ region near the ARM central facility (35.6°–37.6°N, 96.5°–98.5°W). To study the potential impact of the SZA, data collected over an extended period (March–August 1994) were analyzed for each SZA interval of 10°. It is obvious from Fig. 13 that the two sets of measurements correspond much more closely than between ScaRaB and GOES data. This is understandable since the two ScaRaB detectors have the same FOVs and are scanned in the same manner simultaneously. Obviously, the broadband albedo is correlated linearly with visible albedo. The linearity of the relationship is consistent with many previous investigations (Minnis and Harrison 1984; Wydick et al. 1987; Li and Leighton 1992; Vesperini and Fouquart 1994). The slope and intercept of the linear regression depend moderately on SZA, a new feature of the conversion that was not taken into account in previous studies. The following regression equation was derived from the data shown in Fig. 13:

$$\alpha_{SW} = [7.636 - 2.549 \ln(\mu_0) - 1.469 \ln^2(\mu_0)] + \alpha_{VIS}[0.753 - 0.00082 \ln(\mu_0) + 0.0288 \ln^2(\mu_0)], \quad (3)$$

where α_{SW} and α_{VIS} denote broadband SW and visible albedos, respectively. The μ_0 is the cosine of the SZA. The conversion relationships used for generating the *GOES-7* broadband albedo are given below (Minnis et al. 1995):

$$\alpha_{SW} = \alpha_{SW}(CLR)(1 - n) + \alpha_{SW}(CLD)n, \quad (4)$$

$$\alpha_{SW}(CLR) = a_0 + a_1\alpha_{VIS}(CLR) + a_2 \ln(1/\mu_0), \quad (5)$$

and

$$\alpha_{SW}(CLD) = b_0 + b_1\alpha_{VIS}(CLD) + b_2\alpha^2_{VIS}(CLD) + b_3 \ln(1/\mu_0), \quad (6)$$

where n is cloud amount; CLR and CLD represent clear and cloudy skies, respectively. The new version of narrowband to broadband conversion applied to *GOES-8* is similar to Eq. (6) but does not require discrimination between cloudy and clear scenes (Smith et al. 1997). Presumably, use of the quadratic equation is a major cause of the trend shown in Fig. 12 in light of the linear relationship found in Fig. 13. Figure 14 depicts the difference in broadband albedo estimated from *GOES-7* using the ScaRaB conversion model [Eq. (3)] and the original one [Eqs. (4) through (6)]. A comparison between Figs. 12 and 14 confirms that inaccurate esti-

mation of the broadband SW albedo from *GOES-7* is due primarily to incorrect narrow- to broadband conversion. While the paper is revised, the GOES product is updated using a modified narrowband to broadband conversion model that is in much better agreement with that derived from ScaRaB but still differs slightly in the slope of the conversion (cf. Fig. 15).

c. *Influence of the conversion on the inference of cloud absorption*

Recently, satellite and surface measurements have been employed synergistically for addressing the impact of clouds on atmospheric absorption (Cess et al. 1995; Li et al. 1995; among others). The ratio of cloud radiative forcing (CRF) at the surface (CRF_{SFC}) and at the TOA (CRF_{TOA}),

$$R = \frac{CRF_{SFC}}{CRF_{TOA}}, \tag{7}$$

has been determined and compared from observations and model output. CRF is defined as the difference between all-sky and clear-sky net fluxes (incoming minus outgoing). While R derived from models is usually around unity, there exists a large discrepancy in the magnitude of R determined from observations, ranging from less than 1.0 to greater than 1.5. The discrepancy greatly impedes our understanding of the ability of clouds to absorb solar radiation and casts doubts on the results of climate modeling.

The surrogate TOA SW radiation product derived from GOES for the ARM is a major data source for addressing this problem (Imre et al. 1996; Smith et al. 1997). Given the deficiencies found above, we recalculated R from the corrected GOES data using the narrow- to broadband conversion derived from ScaRaB observations. Surface measurements for obtaining CRF_{SFC} were made available through the CERES/ARM/GEWEX (Global Energy and Water Cycle Experiment) Experiment (CAGEX) (Charlock and Alberta 1996) for the period of 6–30 April 1994, excluding days 13, 16, 20, 21, 26, and 27. CAGEX compiled a comprehensive database from a variety of ARM observation platforms for validating radiative transfer models. Scene identification needed to determine clear-sky fluxes at both the surface and TOA was based on cloud estimation by Minnis et al. (1995) from GOES. Measurements with a cloud amount less than 0.1% were considered as being clear skies. Surface and TOA net fluxes were averaged, separately, under clear-sky and all-sky conditions from those measurements that are available simultaneously at the surface and TOA. The mean CRF_{TOA} and CRF_{SFC} averaged over the entire data period are -203 W m^{-2} and -218 W m^{-2}, respectively, leading to an R of 1.07. This value is slightly less than those derived from previous versions of the GOES product (Imre et al. 1996; Smith 1997). It agrees more closely with model results and is thus at further odds with the claim of cloud absorption anomaly (Cess et al. 1995). As is implied by the magnitude of R, we found only a small difference in the atmospheric absorptance between all-sky (0.221) and clear-sky (0.194) conditions.

5. Summary

Knowledge of the radiation budget at the TOA is essential to meteorological and climate studies. Due to the gaps between spaceborne radiation missions, TOA radiative fluxes have been inferred from measurements obtained with noncalibrated narrowband radiometers. The quality of these surrogate TOA broadband radiation products needs validation. This study assessed a GOES-based TOA radiation dataset generated for the U.S. Atmospheric Radiation Measurement program (Minnis et al. 1995) by comparing against calibrated measurements obtained from the European ScaRaB.

Discrepancies in spectral filter functions and viewing geometry were accounted for by means of spectral and angular corrections. Scene identification required for these corrections was assessed. Considerable differences exist between the cloud amounts classified by *GOES-7* and ScaRaB. Since the former is more reliable, it replaces the latter for selecting angular dependence models to derive irradiances from radiances. Comparisons were made between *GOES-7* VISSR and ScaRaB data in terms of fluxes, albedos, and brightness temperatures. For narrowband measurements from visible and infrared channels, the two instruments agree well, except for a weak tendency that visible albedos and fluxes from ScaRaB are slightly larger over bright scenes. Comparison of broadband data revealed that the GOES-based estimates of albedos and fluxes are systematically smaller (larger) than ScaRaB measurements for bright (dark) scenes. The difference was attributed to an inaccurate narrowband to broadband conversion. The conversion is linear according to ScaRaB visible and SW measurements, but a quadratic conversion relationship was employed in generating the GOES-based product. This results in an error of approximately 14 W m^{-2} for daytime mean TOA cloud radiative forcing. After removing this caveat, the surface to TOA SW cloud radiative forcing ratio turns out to be 1.07 for April 1994 at the ARM CART site in Oklahoma. This value is in perfect accordance with radiative transfer models. Note that the results presented here are limited to a single region and for a short period of time.

Acknowledgments. A group of scientists led by P. Minnis at the NASA/Langley Research Center are gratefully acknowledged for generating the GOES product used in the study and for numerous discussions. We are indebted to the CNES staff for providing us with the most of the ScaRaB data; and R. Kandel, M. Viollier, and P. Raberanto at Laboratoire de Météorologie Dynamique du CNRS for making available some ScaRaB data. The authors are also thankful to T. Charlock and

T. Alberta for useful discussions and providing CAGEX data. CCRS internal review of the paper was done by G. Fedosejevs. The study was supported partially by the U.S. Department of Energy under Atmospheric Radiation Measurement (ARM) Grant DE-FG02-97ER2361, and benefited from the participation of the science team members of the ScaRaB project.

REFERENCES

Barkstrom, B. R., and G. L. Smith, 1986: The earth radiation budget experiment: Science and implementation. *Rev. Geophys.,* **24,** 379–390.

Bess, T. D., G. L. Smith, R. N. Green, D. A. Rutan, R. S. Kandel, P. Raberanto, and M. Viollier, 1997: Intercomparison of scanning radiometer for radiation budget (ScaRaB) and Earth Radiation Budget Experiment (ERBE) results. Preprints, *Ninth Conf. Atmospheric Radiation,* Long Beach, CA, Amer. Meteor. Soc., 203–207.

Cess, R. D., and Coauthors, 1995: Absorption of solar radiation by clouds: Observations versus models. *Science,* **267,** 496–499.

——, M. H. Zhang, Y. Zhou, X. Jing, and V. Dvortsov, 1996: Absorption of solar radiation by clouds: Interpretation of satellite, surface, and aircraft measurements. *J. Geophys. Res.,* **101,** 23 299–23 309.

Charlock, T. P., and T. L. Alberta, 1996: The CERES/ARM/GEWEX Experiment (CAGEX) for the retrieval of radiative fluxes with satellite data. *Bull. Amer. Meteor. Soc.,* **77,** 2673–2683.

Diekmann, F. J., and G. L. Smith, 1989: Investigation of scene identification algorithms for radiation budget measurements. *J. Geophys. Res.,* **94,** 3395–3412.

Green, R. N., F. B. House, P. W. Stackhouse, X. Wu, S. A. Ackermann, W. L. Smith, and M. J. Johnson, 1990: Intercomparison of scanner and nonscanner measurements for the Earth Radiation Budget Experiment (ERBE). *J. Geophys. Res.,* **95,** 11 785–11 798.

Imre, D. G., E. H. Abramson, and P. H. Daum, 1996: Quantifying cloud-induced shortwave absorption: An examination of uncertainties and recent arguments for large excess absorption. *J. Appl. Meteor.,* **35,** 1991–2010.

Jackobowitz, H., V. Soule, H. L. Kyle, F. B. House, and the ERB *Nimbus-7* Experiment Team, 1984: The Earth Radiation Budget (ERB) experiment: An overview. *J. Geophys. Res.,* **89,** 5021–5038.

Kandel, R. S., J.-L. Monge, M. Viollier, L. A. Pakhomov, V. I. Adas'ko, R. G. Reitenbach, E. Raschke, and R. Stuhlmann, 1994: The ScaRaB project: Earth radiation budget observations from Meteor satellites. *Adv. Space Res.,* **14,** 47–57.

Kneizys, F. X., E. P. Shettle, L. W. Abrieu, J. Chetwynd, G. Anderson, W. Gallery, J. Selby, and S. Clough, 1988: User's Guide to LOWTRAN-7. AFGL-TR-88-0177, AFGL (OPI), Hanscom Air Force Base, MA, 140 pp.

Li, Z., 1996: On the angular correction of satellite radiation measurements: The performance of ERBE angular dependence model in the Arctic. *Theor. Appl. Climatol.,* **54,** 235–248.

——, and H. G. Leighton, 1991: Scene identification and its effect on cloud radiative forcing in the Arctic. *J. Geophys. Res.,* **96,** 9175–9188.

——, and ——, 1992: Narrowband to broadband conversion with spatially autocorrelated reflectance measurements. *J. Appl. Meteor.,* **31,** 421–432.

——, H. W. Barker, and L. Moreau, 1995: The variable effect of clouds on atmospheric absorption of solar radiation. *Nature,* **376,** 486–490.

Masuda, K., H. G. Leighton, and Z. Li, 1995: A new parameterization for the determination of solar flux absorbed at the surface from satellite measurements. *J. Climate,* **8,** 1615–1629.

Minnis, P., and E. F. Harrison, 1984: Diurnal variability of regional cloud and clear-sky radiative parameters derived from GOES data. Part III: November 1978 radiative parameters. *J. Climate Appl. Meteor.,* **23,** 1023–1051.

——, D. F. Young, and E. F. Harrison, 1991: Examination of the relationship between outgoing infrared window and total long-wave fluxes using satellite data. *J. Climate,* **4,** 1114–1133.

——, W. L. Smith, D. P. Garber, J. K Ayers, and D. R. Doelling, 1995: Cloud properties derived from *GOES-7* for spring 1994 ARM intensive observation period using version 1.0.0 of ARM satellite data analysis program. NASA Ref. Publ. 1366, NASA/Langley Research Center, Hampton, VA, 58 pp.

Monge, J.-L., J. Mueller, R. Kandel, and L. A. Pakhomov, 1994: Calibration results: Summary of FM1 parameters. SBRT-6310-RES1-3, 23 pp. [Available from LMD, Ecole Polytechnique, 91128 Palaiseau, Cedex, France.]

Rao, C. R. N., and J. Chen, 1994: Post-launch calibration of the visible and near-infrared channels of the Advanced Very High Resolution Radiometers on *NOAA-7, -9, -11* spacecraft. NOAA Tech. Rep., 22 pp. [Available from NOAA, U.S. Department of Commerce, Washington, DC 20233.]

Raschke, E., T. H. Vonder Haar, W. R. Bandeen, and M. Pasternak, 1973: The annual radiation ballance of the earth–atmosphere system during 1969–70 from *Nimbus-3* measurements. *J. Atmos. Sci.,* **30,** 341–364.

Rossow, W. B., Y. Desormeaux, C. L. Brest, and A. Parker, 1992: International Satellite Cloud Climatology Project (ISCCP). Radiance calibration report. WMO/TD 520, 104 pp. [Available from NASA/Goddard Space Flight Center, Institute for Space Studies, 2880 Broadway, New York, NY 10025.]

——, C. L. Brest, and M. D. Roiter, 1995: International Satellite Cloud Climatology Project (ISCCP). New radiance calibrations. WMO/TD, 736, 71 pp. [Available from NASA/Goddard Space Flight Center, Institute for Space Studies, 2880 Broadway, New York, NY 10025.]

Rutan, D., and T. P. Charlock, 1997: Spectral reflectance, directional reflectance, and broadband albedo of the earth's surface. Preprints, *Ninth. Conf. Atmospheric Radiation,* Long Beach, CA, Amer. Meteor. Soc., 466–470.

Smith, W. L., L. Nguyen, and P. Minnis, 1997: Cloud radiative forcing derived from ARM surface and satellite measurements during ARESE and the spring ARM/UAV IOP. Preprints, *Ninth Conf. Atmospheric Radiation,* Long Beach, CA, Amer. Meteor. Soc., 1–4.

Stephens, G. L., 1978: Radiation profiles in extended water clouds. Part I: Theory. *J. Atmos. Sci.,* **35,** 2111–2122.

Stokes, G. M., and S. E. Schwartz, 1994: The Atmospheric Radiation Measurement (ARM) program: Programmatic background and design of the cloud and radiation test bed. *Bull. Amer. Meteor. Soc.,* **75,** 1201–1221.

Suttles, J. T., and Coauthors, 1988: *Angular Radiation Models for Earth–Atmosphere System. Vol. I—Short-Wave Radiation.* NASA Ref. Publ., 1184, NASA/Langley Research Center, Hampton, VA, 114 pp.

——, B. A. Wielicki, and S. Vemury, 1992: Top-of-atmosphere radiation fluxes: Validation of ERBE scanner inversion algorithms using *Nimbus-7* ERB data. *J. Appl. Meteor.,* **31,** 784–796.

Vesperini, M., and Y. Fouquart, 1994: Determination of broadband short-wave fluxes from the Meteosat visible channel by comparison to ERBE. *Beitr. Phys. Atmos.,* **67,** 121–131.

Viollier, M., R. S. Kandel, and P. Raberanto, 1995: Inversion and space-time-averaging algorithms for ScaRaB (Scanner for Earth Radiation Budget). Comparison with ERBE. *Ann. Geophys.,* **13,** 959–968.

Whitlock, C. H., and Coauthors, 1990: AVHRR and VISSR satellite instrument calibration results for both cirrus and marine stratocumulus IFO periods. FIRE Sci. Rep. NASA CP 3038, NASA/Langley Research Center, Hampton, VA, 451 pp.

Wielicki, B. A., and R. N. Green, 1989: Cloud identification for ERBE radiative flux retrieval. *J. Appl. Meteor.,* **28,** 1133–1146.

——, B. R. Barkstrom, E. F. Harrison, R. B. Lee III, G. L. Smith, and J. E. Cooper, 1996: Clouds and the Earth's Radiant Energy System (CERES): An earth observing system experiment. *Bull. Amer. Meteor. Soc.,* **77,** 853–868.

Wydick, J. E., P. A. Davis, and A. Gruber, 1987: Estimation of broadband planetary albedo from operational narrow-band satellite measurements. NOAA TR/NESDIS 27, 32 pp. [Available from NOAA, U.S. Department of Commerce, Washington, DC 20233.]

Ye, Q., and J. A. Coakley Jr., 1996: Biases in Earth radiation budget observations. Part 2. Consistent scene identification and anisotropic factors. *J. Geopyhys. Res.,* **101,** 21 253–21 263.